Vacuum 125 (2016) 65–74

Contents lists available at ScienceDirect

Vacuum

journal homepage: www.elsevier.com/locate/vacuum

# Gas flow towards an adsorbing planar wall subject to partial gas-surface thermal accommodation

C. Tantos*, S. Naris, D. Valougeorgis

*Laboratory of Transport Phenomena, Department of Mechanical Engineering University of Thessaly, Pedion Areos, 38334 Volos, Greece*

ARTICLE INFO

*Article history:*
Received 8 October 2015
Received in revised form
30 November 2015
Accepted 1 December 2015
Available online 9 December 2015

*Keywords:*
Vacuum gas dynamics
Kinetic modeling
Gas adsorption
Thermal accommodation coefficient
Sticking coefficient

ABSTRACT

The steady half-space single gas flow driven by an adsorbing planar wall is investigated based on the solution of the BGK kinetic model. The mass and heat transfer between the gas and the plate are characterized by the sticking and thermal accommodation coefficients, the surface temperature and the far upstream velocity and temperature. The work is focused on the influence of partial thermal gas-surface interaction on all flow quantities including the sticking coefficient. It has been found that as the gas thermal accommodation on the surface is reduced, for prescribed adsorbing flux and temperature difference, the sticking coefficient must be increased to sustain the prescribed flux or otherwise for the same sticking coefficient the adsorbing flux is reduced. This behavior is enhanced as the difference, between the surface and the far upstream temperatures, is increased. Overall, the effect of the thermal accommodation coefficient is significant in all flow quantities and must be accordingly taken into consideration. The present theoretical/computational investigation of partial thermal accommodation effect may provide a more clear interpretation of measurements of sticking coefficients, and conversely, improve performance calculations for cryopumps.



## 1. Introduction

Gas adsorption processes are present in many natural, physical, biological, and chemical systems and are widely used in industrial applications such as water purification, air conditioning (adsorption chillers), vapor deposition (CD/DVD metallization) and vacuum pumping (getters and cryogenic pumps). Due to mass transfer a gas adsorption flow is induced. Since in most cases the surface temperature is lower (or much lower) than the gas temperature in the bulk flow, heat transfer is also present. Thus, gas adsorption flow combines both mass and heat transfer. At the gas-surface interface a Knudsen layer is developed and therefore, modeling of such flows is commonly based on kinetic theory by applying the Boltzmann equation or kinetic model equations [1] or alternatively the Direct Simulation Monte Carlo Method (DSMC) [2].

In gas adsorption a fraction of molecules impinging to the surface is adsorbed (stick to the surface), while the remaining fraction is re-emitted (reflected) into the gas. At the surface the so-called sticking coefficient is commonly defined as [3].

$$\alpha_{SC} = \frac{J^- - J^+}{J^-}, \tag{1}$$

where $J^-$ and $J^+$ are the particle fluxes impinging to and reflected from the surface respectively. The sticking coefficient $\alpha_{SC} \in [0,1]$ is a measure of the probability that a molecule landing on the surface will permanently stick on it and provides an indication of the effectiveness of gas removal from the system. It may be estimated as a free parameter by matching experimental with corresponding computational results characterizing a specific gas-surface set up (surface porosity, gas type, gas and surface temperatures). Then, these estimates may be applied in deriving boundary conditions for the simulation of adsorption processes in similar set-ups.

Following this procedure the sticking coefficients of several gases for cryopanels coated with activated carbon at very low temperatures have been estimated [4,5] and then, they have been applied in the numerical modeling of cryopumps used in the main pumping systems of magnetic confinement fusion reactors [6,7]. Also, in a recent theoretical work the half-space adsorption flow problem for single gases and gas mixtures has been solved providing the relationship between the problem parameters [8,9]. The problem is solved in dimensionless form based on the DSMC method and it has been found that in the case of single gases the

* Corresponding author.
*E-mail address:* christantos@mie.uth.gr (C. Tantos).

http://dx.doi.org/10.1016/j.vacuum.2015.12.002
0042-207X/

sticking coefficient depends on the Mach number of the flow far upstream and the ratio of the gas temperature far upstream over the surface temperature.

It is noted that all available work is based on the assumption that the emitted particles are in thermal equilibrium with the surface, i.e., the reflected particles have the same temperature with that of the adsorption surface. In cases however, where the temperatures of the surface and of the gas far from the surface differ significantly it is reasonable to argue that the reflected particles are not fully thermally accommodated at the surface. This type of gas-surface thermal interaction is modeled by the so-called thermal accommodation coefficient $\alpha_{TAC}$ [10]. Combining computational and experimental results it has been shown that it varies as $\alpha_{TAC} \in (0,1]$ [10–12], while in light gases may be significantly less than one. For instance in Ref. [11] the measured values of the thermal accommodation coefficient for He and $D_2$ on polished surfaces is about 0.4 and 0.5 respectively. Furthermore, in Ref. [13] it is observed that for light gases the surface roughness effect on the thermal accommodation coefficient is in vicinity only of 10–20%. Thus, it is reasonable to argue that even in rough surfaces imperfect thermal accommodation may occur.

Here, the thermal accommodation coefficient is defined for that fraction of the incident molecular stream which is reflected from the surface [14], i.e.,

$$\alpha_{TAC} = \frac{(1-\alpha_{SC})E^- - E^+}{(1-\alpha_{SC})E^- - E_W^+}. \tag{2}$$

In Eq. (2), $E^-$ is the incident energy flux, $E^+$ is the reflected energy flux and $E_W^+$ is the energy flux that would have been achieved if the reflected molecules were in thermal equilibrium with the surface. For $\alpha_{SC}=0$, the above definition is reduced to the typical one introduced in purely heat transfer problems [10,15]. All above cited works related to adsorption [4–9] have been performed assuming $\alpha_{TAC}=1$.

Here, the steady-state half space single gas adsorption flow, as defined in Ref. [8], is solved via kinetic modeling. The aim of the present work is to investigate the effect of the partial wall thermal accommodation $\alpha_{TAC} \in [0,1]$ on the other flow parameters and mainly on the sticking coefficient $\alpha_{SC}$. Furthermore, the distributions of all macroscopic quantities with practical interest as well as dimensional results for specific gases are provided. The present work may also support a more clear interpretation of measurements of sticking coefficients, and improve performance calculations for cryopumps.

## 2. Formulation of the gas adsorption flow

Consider an ideal monatomic gas occupying the half space $\hat{x}>0$ bounded by a planar infinite plate located at $\hat{x}=0$, with $\hat{x}$ being the coordinate which spans the direction normal to the plate. The flow setup is shown in Fig. 1. The gas motion is generated by the adsorbing plate maintained at uniform temperature $T_W$, while the mass and heat transfer between the gas and the plate are characterized by the sticking coefficient $\alpha_{SC}$ and thermal accommodation coefficient $\alpha_{TAC}$. Far upstream the gas is at local equilibrium at some temperature $T_\infty \geq T_W$ flowing with some velocity $U_\infty$ in the negative $\hat{x}$ direction. As shown in Fig. 1, the flow is one-dimensional normal to the plate. The molecular velocity vectors $\hat{\boldsymbol{c}} = [\hat{c}_x, \hat{c}_y, \hat{c}_z]$, with $\hat{c}_x<0$ and $\hat{c}_x>0$ refer to incoming and outgoing particles. In spite of the simplicity of the flow configuration the relationship among the flow parameters and their effect on the flow bulk quantities have not been yet fully investigated.

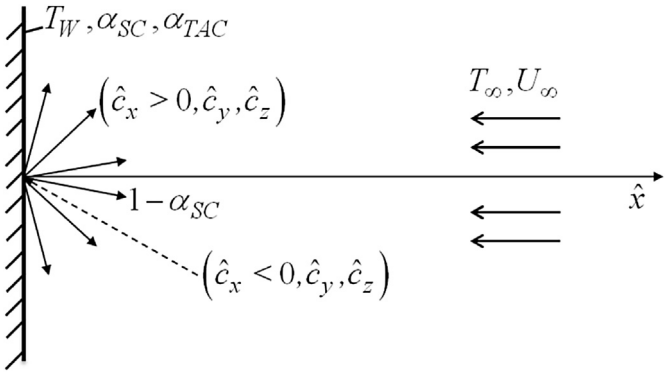


**Fig. 1.** Half-space flow configuration.

### 2.1. Basic equations

The adsorption flow is governed by the steady-state one-dimensional Bhatnagar-Gross-Krook (BGK) kinetic equation [16,17] given by

$$\xi_x \frac{\partial \hat{f}}{\partial \hat{x}} = \nu\left(\hat{f}^M - \hat{f}\right). \tag{3}$$

Here, the main unknown is the distribution function $\hat{f} = \hat{f}(\hat{x}, \hat{\boldsymbol{c}})$, with $\hat{\boldsymbol{c}} = [\hat{c}_x, \hat{c}_y, \hat{c}_z]$ being the molecular velocity vector, $\nu = P/\mu$, where $P$ is the local pressure and $\mu$ is the viscosity at local temperature $T$, is the collision frequency and

$$\hat{f}^M = \frac{N}{(2\pi RT)^{3/2}} \exp\left[-\frac{(\hat{c}_x - U)^2 + \hat{c}_y^2 + \hat{c}_z^2}{2RT}\right] \tag{4}$$

is the local Maxwellian distribution, with $R$ denoting the gas constant. Also, the number density $N$, the $\hat{x}-$ component of the bulk velocity $U$ (the other two components are zero) and temperature $T$ are defined by the moments of $\hat{f}$ as follows:

$$N(\hat{x}) = \int_{-\infty}^{\infty}\int_{-\infty}^{\infty}\int_{-\infty}^{\infty} \hat{f}\, d\hat{c}_x d\hat{c}_y d\hat{c}_z \tag{5}$$

$$U(\hat{x}) = \frac{1}{N(\hat{x})}\int_{-\infty}^{\infty}\int_{-\infty}^{\infty}\int_{-\infty}^{\infty} \hat{c}_x \hat{f}\, d\hat{c}_x d\hat{c}_y d\hat{c}_z \tag{6}$$

$$T(\hat{x}) = \frac{1}{3N(\hat{x})R}\int_{-\infty}^{\infty}\int_{-\infty}^{\infty}\int_{-\infty}^{\infty} \left[(\hat{c}_x - U)^2 + \hat{c}_y^2 + \hat{c}_z^2\right]\hat{f}\, d\hat{c}_x d\hat{c}_y d\hat{c}_z \tag{7}$$

Other macroscopic quantities of some practical interest in the present work are the pressure defined by the equation of state $P = Nk_BT$, where $k_B$ is the Boltzmann constant, the normal pressures

$$P_{xx}(\hat{x}) = m\int_{-\infty}^{\infty}\int_{-\infty}^{\infty}\int_{-\infty}^{\infty} (\hat{c}_x - U)^2 \hat{f}\, d\hat{c}_x d\hat{c}_y d\hat{c}_z, \quad P_{yy}(\hat{x}) = P_{zz}(\hat{x}) = m\int_{-\infty}^{\infty}\int_{-\infty}^{\infty}\int_{-\infty}^{\infty} \hat{c}_y^2 \hat{f}\, d\hat{c}_x d\hat{c}_y d\hat{c}_z \tag{8}$$

and the energy and heat fluxes in the $x$ direction given by

$$E(\hat{x}) = \frac{m}{2}\int_{-\infty}^{\infty}\int_{-\infty}^{\infty}\int_{-\infty}^{\infty}\hat{c}^2\hat{c}_x\hat{f}\,d\hat{c}_x d\hat{c}_y d\hat{c}_z \tag{9}$$

and

$$Q(\hat{x}) = \frac{m}{2}\int_{-\infty}^{\infty}\int_{-\infty}^{\infty}\int_{-\infty}^{\infty}\left[(\hat{c}_x-U)^2+\hat{c}_y^2+\hat{c}_z^2\right](\hat{c}_x-U)\hat{f}\,d\hat{c}_x d\hat{c}_y d\hat{c}_z, \tag{10}$$

respectively, where $m$ is the molecular mass ($R = k_B/m$).

As it is well known correct expressions for both viscosity and thermal conductivity cannot be proved simultaneously based on the BGK approximation. In spite of this pitfall and its simplicity it has been numerically demonstrated that it is a very reliable model for solving nonisothermal flows deducing results which are very close to the corresponding ones obtained by solving other kinetic models, the Boltzmann equation and the DSMC method [18,19]. Therefore it has been also implemented in the present work producing, as shown in Section 3.1, very accurate results with the minimum computational effort.

It is convenient to rewrite the governing equations in dimensionless form using the far upstream ($\hat{x}\to\infty$) macroscopic distributions as reference quantities. Thus, the dimensionless number density, velocity, temperature, normal stresses, pressure, energy flux and heat flux are defined as

$$\begin{aligned} &n = N/N_\infty, \quad u = U/v_\infty, \quad \tau = T/T_\infty, \quad p_{ii} = P_{ii}/(2P_\infty),\\ &p = P/P_\infty, \quad e = E/(P_\infty v_\infty), \quad q = Q/(P_\infty v_\infty)\end{aligned} \tag{11}$$

respectively. All quantities with the subscript "$\infty$" are the reference quantities, with $v_\infty = \sqrt{2RT_\infty}$ being the most probable molecular speed far upstream. The equation of state now reads $p = n\times\tau$. The equivalent mean free path far upstream, defined as [20,21].

$$\lambda_\infty = \frac{2}{\sqrt{\pi}}\frac{\mu_\infty v_\infty}{P_\infty}, \tag{12}$$

is taken as the characteristic length. The dimensionless distribution function is given by $f(x,\boldsymbol{c}) = \hat{f}(\hat{x},\hat{\boldsymbol{c}})v_\infty^3/N_\infty$, where $x = \hat{x}/\lambda_\infty$ and $\boldsymbol{c} = \hat{\boldsymbol{c}}/v_\infty$ are the dimensionless length and molecular velocity vector respectively.

Furthermore, the computational effort is significantly reduced by eliminating, based on the well-known projection procedure, the $y-$ and $z-$ components of the molecular velocity vector $\boldsymbol{c} = [c_x,c_y,c_z]$. This is achieved by introducing the reduced distributions [22]:

$$\begin{aligned} F(x,c_x) &= \int_{-\infty}^{\infty}\int_{-\infty}^{\infty} f dc_y dc_z \quad \text{and}\\ G(x,c_x) &= \int_{-\infty}^{\infty}\int_{-\infty}^{\infty}\left(c_y^2+c_z^2\right) f dc_y dc_z.\end{aligned} \tag{13}$$

Next, operating successively on the dimensionless form of Eqs. (3)–(10) with the integral operators $\int_{-\infty}^{\infty}\int_{-\infty}^{\infty}(\cdot)dc_z dc_y$ and $\int_{-\infty}^{\infty}\int_{-\infty}^{\infty}(\cdot)(c_y^2+c_z^2)dc_z dc_y$, yields a system of two integro-differential equations for the reduced distributions functions

$$c_x\frac{\partial F}{\partial x} = \frac{2}{\sqrt{\pi}}\rho\sqrt{\tau}\left[F^M - F\right], \quad c_x\frac{\partial G}{\partial x} = \frac{2}{\sqrt{\pi}}\rho\sqrt{\tau}\left[G^M - G\right] \tag{14}$$

with the reduced Maxwellians given by

$$\begin{aligned} F^M &= \frac{\rho}{(\pi\tau)^{1/2}}\exp\left[-\frac{(c_x-u_x)^2}{\tau}\right],\\ G^M &= \frac{\rho\tau}{(\pi\tau)^{1/2}}\exp\left[-\frac{(c_x-u_x)^2}{\tau}\right]\end{aligned} \tag{15}$$

coupled with the associated moments

$$\begin{aligned} &n(x) = \int_{-\infty}^{\infty} F dc_x,\ u(x) = \frac{1}{n}\int_{-\infty}^{\infty} c_x F dc_x,\\ &\tau(x) = \frac{2}{3n}\int_{-\infty}^{\infty}\left[(c_x-u)^2F+G\right]dc_x,\ P_{xx}(x) = \int_{-\infty}^{\infty}(c_x-u)^2 F dc_x,\\ &E(x) = \int_{-\infty}^{\infty} c_x\left(c_x^2F+G\right)dc_x,\ q_x(x) = \int_{-\infty}^{\infty}(c_x-u)\left[(c_x-u)^2F+G\right]dc_x.\end{aligned} \tag{16}$$

In the formulation of the basic equation (14) the hard-sphere (HS) intermolecular interaction model has been applied.

### 2.2. Boundary conditions

The adsorption process on the planar surface at $\hat{x} = 0$ is modeled by prescribing the distribution of reflected molecules according to

$$\hat{f}(0,\boldsymbol{c}) = \frac{N_W}{(2\pi RT_A)^{3/2}}\exp\left(-\frac{\hat{c}_x^2+\hat{c}_y^2+\hat{c}_z^2}{2RT_A}\right), \quad \hat{c}_x > 0, \tag{17}$$

where the parameters $N_W$ and $T_A$ may be defined as follows.

The parameter $N_W$ is specified by substituting Eq. (17) into the expression of the reflected particle flux $J^+ = \int_{\hat{c}_x>0}\hat{c}_x\hat{f}(0,\hat{\boldsymbol{c}})d\hat{\boldsymbol{c}}$ to deduce $J^+ = N_W\sqrt{RT_A}/\sqrt{2\pi}$. In this expression the definition of the sticking coefficient given by Eq. (1) is introduced, to find

$$N_W = (1-\alpha_{SC})\sqrt{\frac{2\pi}{RT_A}}J^-, \tag{18}$$

where $J^- = -\int_{\hat{c}_x<0}\hat{c}_x\hat{f}(0,\hat{\boldsymbol{c}})d\hat{\boldsymbol{c}}$ is the incident particle flux.

The parameter $T_A$, which has been introduced in the boundary condition in order to take into account partial thermal accommodation, is defined by substituting Eq. (17) into the expression for the reflected energy flux $E^+ = \frac{m}{2}\int_{\hat{c}_x>0}\hat{c}_x\hat{c}^2\hat{f}\ (0,\hat{\boldsymbol{c}})\ d\hat{\boldsymbol{c}}$. In the resulting expression, Eq. (18) is introduced to yield $E^+ = 2(1-\alpha_{SC})J^-k_BT_A$. Operating similarly in the case of full thermal accommodation (now $T_A$ is replaced by $T_W$) is readily deduced that $E_W^+ = 2(1-\alpha_{SC})J^-k_BT_W$. These two expressions for $E^+$ and $E_W^+$ are substituted into Eq. (2) for the thermal accommodation coefficient to find

$$T_A = \alpha_{TAC}T_W + (1-\alpha_{TAC})\frac{E^-}{2k_BJ^-} \tag{19}$$

where $E^- = -\frac{m}{2}\int_{\hat{c}_x<0}\hat{c}_x\hat{c}^2\hat{f}(0,\hat{\boldsymbol{c}})d\hat{\boldsymbol{c}}$ is the incident energy flux. Thus, boundary condition (17) for the reflected molecules is fully defined in terms of the impinging distribution, which is part of the

solution.

Far upstream ($\hat{x}\to\infty$) the gas flow is described by a Maxwellian written as

$$\hat{f}_\infty(\hat{\boldsymbol{c}}) = \frac{N_\infty}{(2\pi RT_\infty)^{3/2}}\exp\left(-\frac{(\hat{c}_x-U_\infty)^2+\hat{c}_y^2+\hat{c}_z^2}{2RT_\infty}\right). \tag{20}$$

At that end the distribution function and the resulting macroscopic quantities should not depend on the spatial variable $\hat{x}$.

Next, the boundary conditions are non-dimensionalized and the projection procedure is introduced in the same manner as in the basic equations. Following this routine manipulation at $x=0$ the emitted reduced distributions are

$$\begin{aligned} F(0,c_x) &= \frac{n_W}{\sqrt{\pi\tau_A}}\exp\left[-\frac{c_x^2}{\tau_A}\right],\\ G(0,c_x) &= \frac{n_W\sqrt{\tau_A}}{\sqrt{\pi}}\exp\left[-\frac{c_x^2}{\tau_A}\right], \quad c_x>0 \end{aligned} \tag{21}$$

where the parameters are given by

$$n_W = (1-\alpha_{SC})\frac{2\sqrt{\pi}}{\sqrt{\tau_A}}j^-, \quad \tau_A = \alpha_{TAC}\tau_W + (1-\alpha_{TAC})\frac{e^-}{2j^-}, \tag{22}$$

with the incident particle and energy fluxes computed as

$$\begin{aligned} j^- &= -\int_{c_x<0} c_x F(0,c_x)dc_x,\\ e^- &= -\int_{c_x<0} c_x\left[c_x^2F(0,c_x)+G(0,c_x)\right]dc_x, \end{aligned} \tag{23}$$

while at $\hat{x}\to\infty$ the Maxwellian takes the form

$$F_\infty = G_\infty = \frac{1}{\sqrt{\pi}}\exp\left[-(c_x-u_\infty)^2\right]. \tag{24}$$

In Eqs. (21)–(24), the dimensionless quantities are $n_W = N_W/N_\infty$, $u_\infty = U_\infty/v_\infty$, $\tau_A = T_A/T_\infty$, $\tau_W = T_W/T_\infty$, $j^- = J^-/(v_\infty N_\infty)$ and $e^- = E^-/(P_\infty v_\infty)$.

Based on the above dimensionless formulation the flow parameters involved in the present one-dimensional adsorption flow problem are four, namely the coefficients $\alpha_{SC}$ and $\alpha_{TAC}$, the temperature ratio $\tau_W$ and the velocity $u_\infty$. Commonly, the dimensionless velocity at infinity $u_\infty$ is presented via the Mach number far upstream defined as $Ma_\infty = |U_\infty|/c_\infty$, where $c_\infty = \sqrt{\gamma RT_\infty}$ is the corresponding sound speed [8]. Since for a monatomic gas the ratio of the specific heats is $\gamma = 5/3$ it is seen that $Ma_\infty = |u_\infty|\sqrt{6/5}$.

### 2.3. Numerical scheme

The governing equation (14) with the associated expressions (15) and (16) subject to boundary conditions (21)–(24) are solved numerically in an iterative manner. More specifically for prescribed values of $\alpha_{SC}$, $\alpha_{TAC}$ and $\tau_W$ the iteration map starts by assuming all needed macroscopic quantities including the far upstream velocity $u_\infty$ as well as the parameters $n_W$ and $\tau_A$. The kinetic equation (14) are solved to yield the reduced distributions $F$ and $G$, which are introduced into the moment equation (16) as well as in the flux equation (23) to find the new estimates of all bulk quantities which are now introduced in the next iteration. The iteration process is terminated when the imposed convergence criteria is fulfilled. Upon convergence the correct value of $u_\infty$ is recovered. Thus, the present problem is properly defined only when three out of the four involved parameters are given. If all parameters both at the plane surface and far upstream are defined no steady-state flow conditions may be reached. Here, we have chosen to compute $u_\infty$ (or the associated Mach number $Ma_\infty$) as a function of the remaining three parameters, i.e.,

$$u_\infty = u_\infty(\alpha_{SC},\alpha_{TAC},\tau_W) \tag{25}$$

The discretization of the kinetic equations in the molecular velocity space is based on the discrete velocity method. In the physical space a second order control volume approach is applied using non-uniform grid spacing which follows the geometric sequence $\Delta x_i = \Delta x_1 \times r^{i-1}$, with $\Delta x_1 = 4\times10^{-7}$ and $r = 1.0009$ (the subscript $i = 1, ..., K$ refers to the nodes in the physical space). The macroscopic quantities are computed by Gauss quadrature. This numerical scheme has been extensively applied in the solution of rarefied gas flows with considerable success [23]. The results presented in the next section have been obtained with about 15,000 nodes in the physical space and 16 molecular speeds, while the convergence criteria to be fulfilled is

$$\frac{1}{3K}\sum_{i=1}^{K}\left[\left|n_i^{(t+1)}-n_i^{(t)}\right|+\left|\tau_i^{(t+1)}-\tau_i^{(t)}\right|+\left|u_i^{(t+1)}-u_i^{(t)}\right|\right]<\varepsilon. \tag{26}$$

In (26) the superscript $t$ denotes the iteration index and $\varepsilon = 10^{-5}$ is the tolerance parameter. For the most time intensive cases (small values of $\alpha_{SC}$) the computing time associated to a serial BGK simulation with the prescribed numerical parameters on a laptop equipped with Intel® Core™ i5-3570 CPU (3.40 GHz) is about 300 min. For $\alpha_{SC}=0$ the solution of the corresponding half-space purely heat transfer solution is recovered.

## 3. Results and discussion

A validation of the modeling approach and of the accuracy of the results is displayed in Section 3.1. In Section 3.2, results are presented and discussed for the macroscopic velocity and the Mach number far upstream, as well as for the half space distributions of density, velocity, temperature and pressure in terms of the sticking and thermal accommodation coefficients varying between zero and one and for typical values of the temperature ratio $\tau_W = T_W/T_\infty$. The

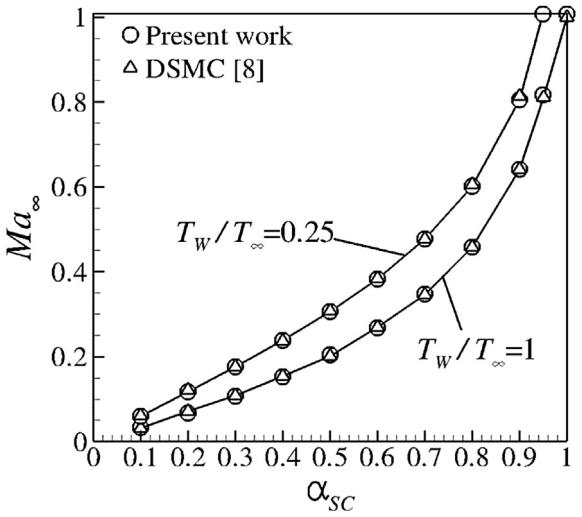


**Fig. 2.** Upstream Mach number $Ma_\infty$ as a function of the sticking coefficient $\alpha_{SC}$ for thermal accommodation coefficient $\alpha_{TAC}=1$ and temperature ratio $\tau_W = T_W/T_\infty = [1,0.25]$ based on the present kinetic model and the DSMC method [8].

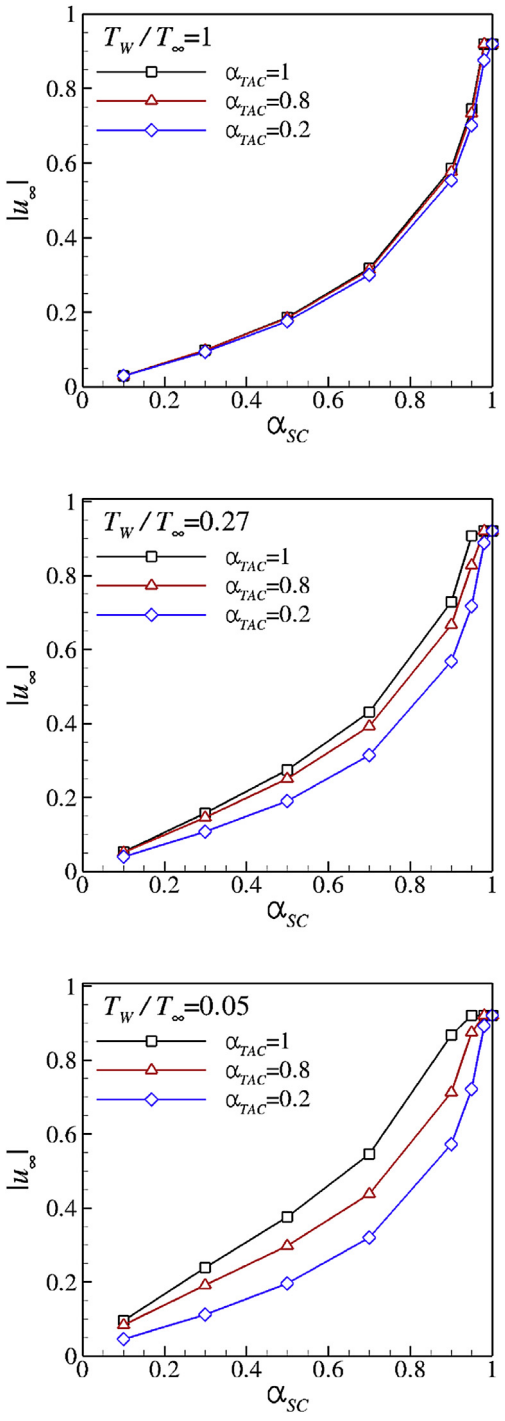


**Fig. 3.** Upstream velocity $|u_\infty|$ as a function of the sticking coefficient $\alpha_{SC}$ for thermal accommodation coefficient $\alpha_{TAC}=[1,0.8,0.2]$ and temperature ratio $\tau_W=T_W/T_\infty=[1,0.27,0.05]$.

dependency of the thickness of the Knudsen layer on the flow parameters and the inclusion of an effective wall temperature to approximately compensate the thermal accommodation effect are also discussed. Finally, in Section 3.3 some dimensional results for specific gases are presented.

At this point it is useful to note that since the upstream quantities are taken as the reference quantities, $n_\infty = 1$ and thus $|u_\infty| = j_\infty = \alpha_{SC} j^-$, i.e. is equal to the upstream net particle flux and to the adsorbed particle flux (all in dimensionless form) and therefore characterizes the intensity of the adsorption process.

### 3.1. Benchmarking

The accuracy of the results has been confirmed in several ways. In all cases the length $L$ of the computational domain, i.e., the distance between the plate and the position on the $x-$ axis, where the far upstream boundary condition is imposed, has been computationally checked to be long enough to properly recover space independent quantities at that end. Several runs have been performed for the same set of parameters by increasing $L$ until no variation in the numerical results is observed. Grid independency of the results is also confirmed. Furthermore, in all cases tested, the computed macroscopic distributions fulfill the conservation laws derived in the Appendix. Based on the prescribed numerical parameters, convergence of the results up to at least three significant figures is confirmed.

To further validate the accuracy of the results a comparison with available corresponding results in the literature is performed. As it is pointed in the introduction, the same flow configuration has been studied in Ref. [8] for $\alpha_{TAC}=1$ based on the DSMC method. In Fig. 2, which reports the upstream Mach number $Ma_\infty$ versus $\alpha_{SC}$, a comparison is performed between the results of the present work and the corresponding ones in Ref. [8] for $\tau_W=T_W/T_\infty=1$ and 0.25. It is clearly seen that although the two computational approaches are completely different (the present one is deterministic, while the one in Ref. [8] is stochastic) the agreement between the results in the whole range of the sticking coefficient and for both temperature ratios is excellent with the relative error being less than 1%. Also, as shown in Fig. 2, increasing the $Ma_\infty$ leads to higher values of $\alpha_{SC}$. In addition, as $\tau_W$ is reduced, i.e., the temperature difference between the upstream gas and surface temperatures $\Delta T=T_\infty-T_W$ is increased, for the same $\alpha_{SC}$, the $Ma_\infty$ is increased, which means that the adsorption process becomes more intense. This remark may be alternatively stated by saying that as $\tau_W$ is reduced, for the same $Ma_\infty$, a lower $\alpha_{SC}$ is needed in the specific adsorption processes. As expected the effect of $\Delta T$ is important.

### 3.2. Effect of partial thermal accommodation

Next, we focus to the main objective of the present work which is the investigation of the effect of $\alpha_{TAC}$ on the adsorption process. In Fig. 3, the magnitude of the computed far upstream velocity $u_\infty$ is plotted as a function of $\alpha_{SC}$ for $\alpha_{TAC}=[1,0.8,0.2]$ and $\tau_W=T_W/$

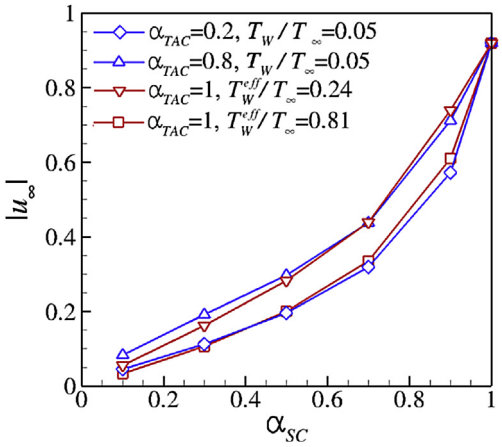


**Fig. 4.** Comparison between the results obtained by using the ratio $T_W^{eff}/T_\infty=[0.24,0.81]$ and $\alpha_{TAC}=1$ with the corresponding "exact" ones.

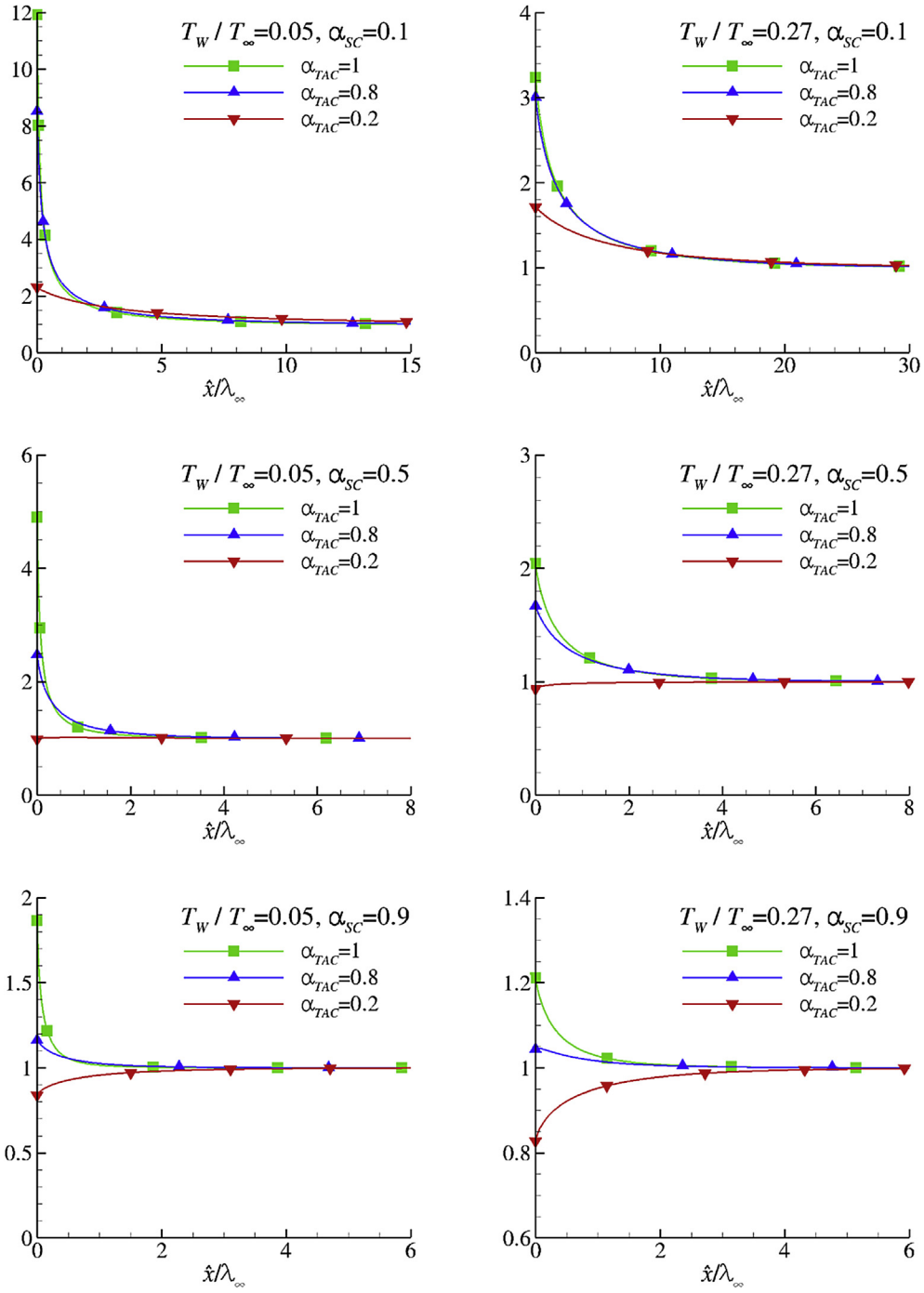


**Fig. 5.** Dimensionless number density $n(x)$ for temperature ratios $\tau_W = T_W/T_\infty = [0.05,0.27]$ with sticking coefficient $\alpha_{SC} = [0.1,0.5,0.9]$ and thermal accommodation coefficient $\alpha_{TAC} = [1,0.8,0.2]$.

$T_\infty = [1,0.27,0.05]$. For $\tau_W = 1$, the effect of $\alpha_{TAC}$ is negligible. This is well expected since when the surface and upstream temperatures are equal there is no heat transfer mechanism. However, as $\tau_W$ is reduced (the temperature difference is increased) heat transfer is enhanced and as a result the effect of $\alpha_{TAC}$ is also increased. In general, $|u_\infty|$ is reduced as $\alpha_{TAC}$ is reduced, i.e., as the gas thermal accommodation at the plate becomes less complete. This is physically justified since, in practice, a lower thermal accommodation at the surface corresponds (at some sense) to some smaller temperature difference $\Delta T$ than the imposed one. Indicatively, at fixed values of $\alpha_{SC} = 0.7$ and $\tau_W = 0.27$, when $\alpha_{TAC} = 0.8$ and 0.2, the reductions in $|u_\infty|$, compared to the ones for $\alpha_{TAC} = 1$, are 9% and 27% respectively. The corresponding reductions at $\tau_W = 0.05$ are 20% and 42%. Also, for prescribed adsorbing flux and temperature difference, as $\alpha_{TAC}$ is reduced, the sticking coefficient must be increased to sustain the prescribed flux. For instance in the case of $\tau_W = 0.05$, when $\alpha_{TAC}$ is reduced from 1 to 0.2, in order to preserve $|u_\infty| \simeq 0.6$ the sticking coefficient is increased about 25%. The effect of $\alpha_{TAC}$ becomes more important at low and intermediate values of $\alpha_{SC}$ between 0.1 and 0.8. Overall, the effect of $\alpha_{TAC}$ is of similar importance with $\tau_W$.

It is noted that the specific temperature ratios of 0.27 and 0.05

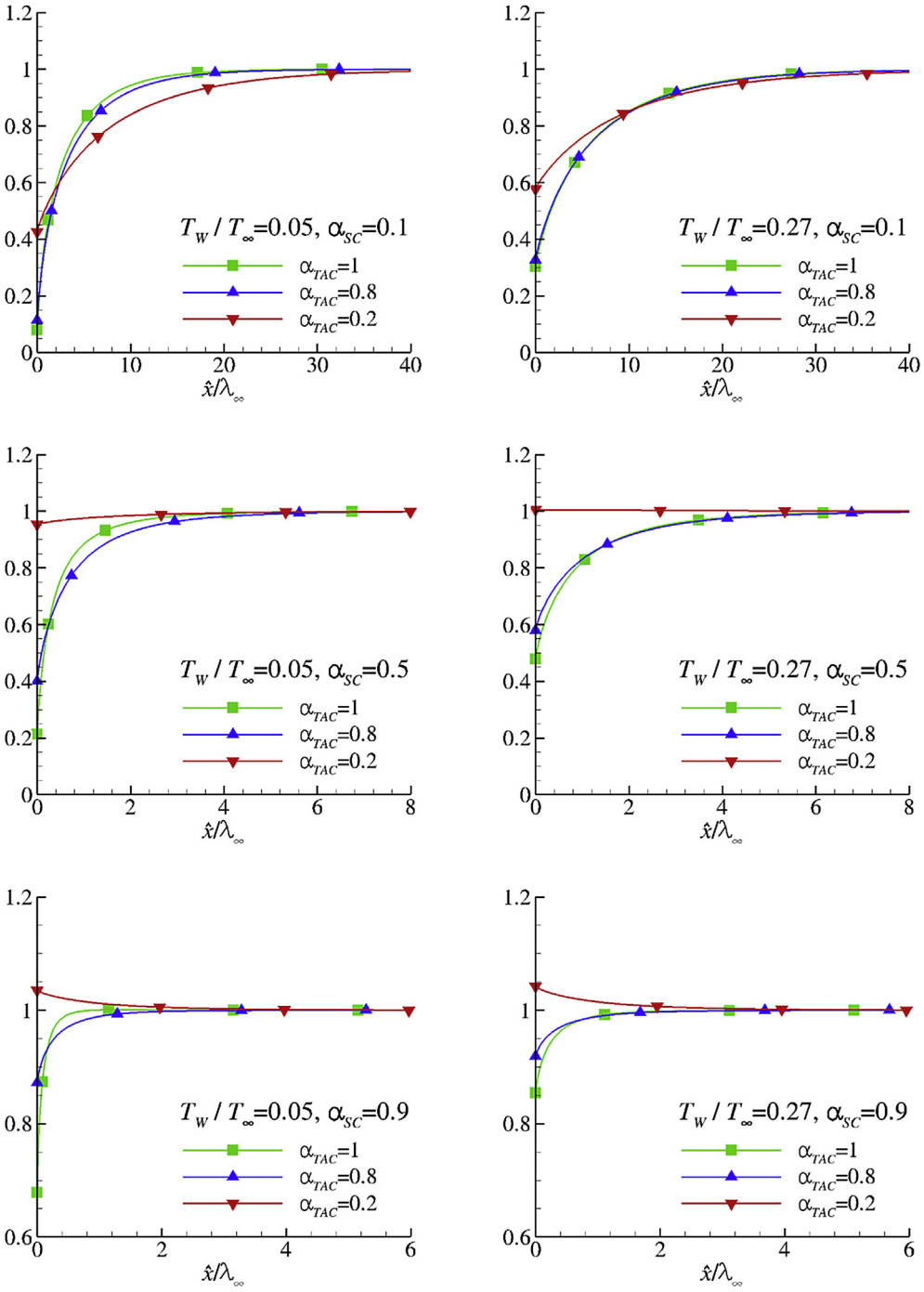


**Fig. 6.** Dimensionless temperature $\tau(x)$ for temperature ratios $\tau_W = T_W/T_\infty = [0.05,0.27]$ with sticking coefficient $\alpha_{SC} = [0.1,0.5,0.9]$ and thermal accommodation coefficient $\alpha_{TAC} = [1,0.8,0.2]$.

have been selected because, for $T_\infty = 300$ K, they correspond to $T_W = 80$ K and 15 K respectively, which are two typical temperatures in the design of multistage cryopumps [24] including the design of a three-stage cryopump which is recently under consideration within the EUROfusion programme [25]. Of course, they are also indicative for other temperature ratios covering a wide range of temperature differences.

Based on the results of Fig. 3 it may be useful to attempt to compensate the effect of $\alpha_{TAC} < 1$ by introducing an effective wall temperature $T_W^{eff} > T_W$ associated always with perfect thermal accommodation ($\alpha_{TAC} = 1$). It should be like a weighted average temperature and therefore it is defined as

$$T_W^{eff} = \alpha_{TAC} T_W + (1 - \alpha_{TAC}) T_\infty. \tag{27}$$

In Fig. 4, the magnitude of the computed far upstream velocity $|u_\infty|$ is plotted as a function of $\alpha_{SC}$ for $T_W^{eff}/T_\infty = 0.81$ and 0.24 with $\alpha_{TAC} = 1$. In the same figure the corresponding results for $T_W/T_\infty = 0.05$ with $\alpha_{TAC} = 0.2$ and 0.8, which are the parameters used to obtain the two specific values of $T_W^{eff}/T_\infty$, are also plotted for comparison purposes. In general the agreement is good at high and moderate values of $\alpha_{SC}$ and it deteriorates as $\alpha_{SC}$ is further

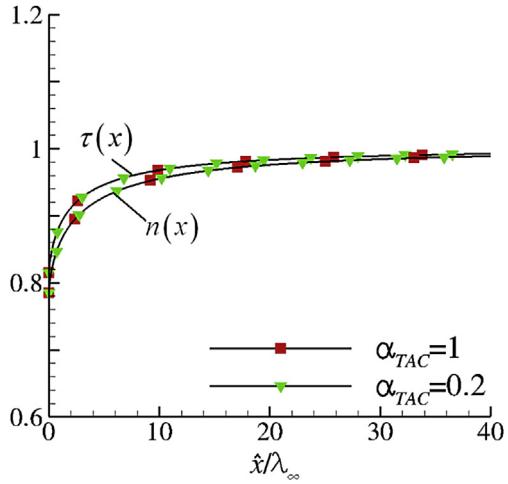


**Fig. 7.** Dimensionless number density $n(x)$ and temperature $\tau(x)$ for temperature ratio $\tau_W = T_W/T_\infty = 0.05$ with sticking coefficient $\alpha_{SC} = 1$ and thermal accommodation coefficient $\alpha_{TAC} = [1,0.2]$.

decreased. At $\alpha_{SC} = 0.1$ the disagreement is about 30%. In general the effective temperature approach may be useful for practical applications when computational resources are limited.

A more detailed insight in the adsorption flow characteristics is displayed in Figs. 5 and 6, where the dimensionless distributions of number density and temperature are displayed for two temperature ratios $\tau_W = [0.05,0.27]$ with the sticking and thermal accommodation coefficients taking the typical values of $\alpha_{SC} = [0.1,0.5,0.9]$ and $\alpha_{TAC} = [0.2,0.8,1]$ respectively. In all cases the distance along the horizontal axis from the plate is in mean free paths and the total indicated length corresponds to the length $L$ of the computational domain. This length also corresponds to the thickness of the adsorption Knudsen layer where non-equilibrium transport phenomena occur. As shown in Figs. 5 and 6, it is influenced from both $\alpha_{SC}$ and $\tau_W$. It is evident that increasing the sticking coefficient $\alpha_{SC}$ leads to lower values of $L$, which means that the far upstream conditions are recovered faster in a smaller number of mean free paths $\hat{x}/\lambda_\infty$ from the adsorption surface. The effect of the temperature difference is not that clear but it has been observed that decreasing $\tau_W$ reduces the thickness $L$.

In Fig. 5, the number density profile $n(x)$ is plotted. The shape of $n(x)$ is qualitatively similar for both $\tau_W = 0.05$ and 0.27. However, in the former case (i.e. as the plate temperature is decreased), it is changing more rapidly reaching to higher number densities at the plate. The far upstream number density is (as it should) always equal to one. For $\alpha_{TAC} = 1$ and 0.8, as $x$ is reduced, for all values of $\alpha_{SC}$, the number densities are monotonically increased reaching their highest values on the surface ($x = 0$). In particular, for $\alpha_{SC} = 0.1$ the two profiles are very close and then for $\alpha_{SC} = 0.5$ and 0.9 there is a departure between the profiles with the number density taking lower values as the sticking coefficient is increased. This behavior remains the same for $\alpha_{TAC} = 0.2$ and $\alpha_{SC} = 0.1$. On the contrary for $\alpha_{TAC} = 0.2$ and $\alpha_{SC} = 0.5$ and 0.9, as $x$ is reduced, the number densities are monotonically reduced reaching their lowest values at $x = 0$. Overall, increasing the sticking coefficient leads to lower values of density. For low enough values of $\alpha_{TAC}$ the number density is even lower than the far upstream value. This behavior in terms of the thermal accommodation is physically explained since, as pointed out above, as $\alpha_{TAC}$ is decreased the gas is reflected from the surface with a temperature larger than the surface temperature and as a result the gas density is decreased.

The corresponding dimensionless temperature profiles $\tau(x)$ are displayed in Fig. 6. The gas temperature far upstream is equal to one and then in most cases, as expected, the temperature is monotonically decreased approaching to the adsorption surface. This situation is reversed only at $\alpha_{SC} = 0.9$ and 0.5 combined with $\alpha_{TAC} = 0.2$, resulting to gas temperatures close to the plate higher than the far upstream ones. It may be justified by considering that the thermal energy transferred by the reflected particles at the wall may be larger than the corresponding amount of particles at some location far from the wall and therefore, it appears only for $\alpha_{SC} < 1$ and it is enhanced as both $\Delta T = T_\infty - T_W$ and $\alpha_{TAC}$ are decreased.

Other macroscopic quantities of some practical interest are the velocity and pressure distributions. As shown in the Appendix the particle flux conservation law $n(x)u(x) = u_\infty$ or $n(x)u(x)/u_\infty = 1$ applies. Thus, the behavior of the normalized velocity magnitude $|u(x)/u_\infty|$ is the reciprocal of the one observed for the number density. Furthermore, the variation of pressure along the $x-$ axis may be obtained from the equation of state $p(x) = n(x)\tau(x)$. It is also noted that the behavior of the normal pressure $p_{xx}(x)$ is similar to $p(x)$, while in all cases $p_{yy} = p_{zz}$ and $p_{xy} = p_{xz} = 0$.

The dimensionless density and temperature in the limiting case where $\alpha_{SC} = 1$ are shown in Fig. 7 for $\tau_W = 0.05$ with $\alpha_{TAC} = 1$ and 0.2. As it is seen the solution does not depend on the thermal accommodation coefficient. This is expected, since all particles are adsorbed and there are no reflected particles. Also, both the number density and temperature are monotonically reduced as $x$ is reduced. Comparing these profiles with the corresponding ones for $\alpha_{SC} = 0.9$ and $\alpha_{TAC} = 1$ it is seen that there is a resemblance in temperatures, while the densities behave in an opposite manner (the one for $\alpha_{SC} = 0.9$ is increased as $x$ is reduced).

All simulations reported above are based on the HS model. Corresponding simulations have been performed for the Maxwell intermolecular potential deducing results which are very close to the ones by the HS model. Therefore it is stated that the choice of the intermolecular potential model has negligible effect on the present adsorption flow problem. Another issue of some interest is that corresponding results have been obtained for polyatomic gases based on the Holway model [26]. It has been found that the influence of the internal degrees of freedom is small (about 10%) in this flow configuration and therefore the dimensionless results presented here may be also used in the case of polyatomic gases.

### 3.3. Sticking coefficients of specific gases

Closing this section is useful to provide some results in dimensional form. The dimensionless results presented in Fig. 3 are applied to plot in Fig. 8 the net molar flux in terms of the sticking coefficient for specific monatomic gases namely protium ($^1$H), helium (He), neon (Ne) and xenon (Xe) for reference upstream pressure $P_\infty = 0.1$ Pa and temperature $T_\infty = 300$ K and temperature ratio $T_W/T_\infty = \tau_W = 0.05$. This is easily performed as follows: For the prescribed $P_\infty$ and $T_\infty$ the far upstream number density $N_\infty$ is obtained from the equation of state ($P_\infty = N_\infty k_B T_\infty$). Then, the far upstream velocity is computed as $U_\infty = \upsilon_\infty |u_\infty|$, where $\upsilon_\infty = \sqrt{2k_B T_\infty/m}$ is known for the specific gas and $|u_\infty|$ is obtained from Fig. 2. Finally, the net particle flux is computed as $J_\infty = N_\infty U_\infty$ which is divided by the Avogadro number to be converted into the net molar flux $J_\infty^{(molar)}$ [mol/(m$^2$s)] shown, versus $\alpha_{SC}$ for $\alpha_{TAC} = [0.2,0.8,1]$, in Fig. 8.

It is clearly seen that as the thermal accommodation coefficient is reduced the net molar flux $J_\infty^{(molar)}$, which is equal to the adsorbed molar flux at the surface, is reduced. It is readily deduced, from the above dimensionalization, that the ratio of the net molar fluxes of two gases, for prescribed $\alpha_{SC}$, $\alpha_{TAC}$ and $\tau_W$, is inversely proportional to the square route of their molar masses. Thus, it is stated that under the same prescribed reference conditions and coefficients,

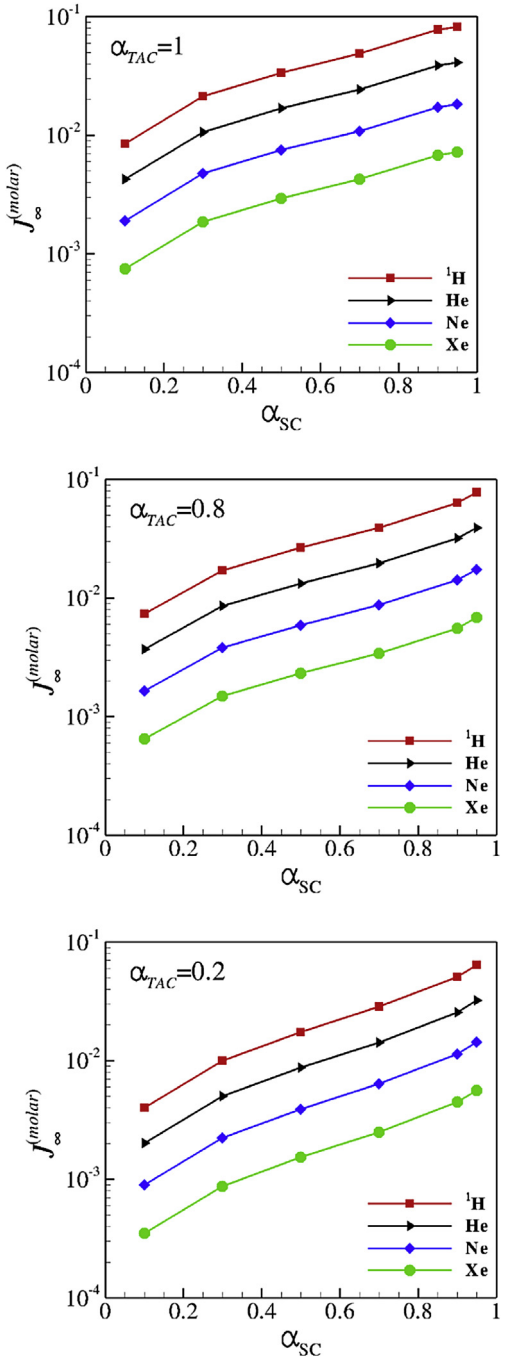


**Fig. 8.** Net molar flux $J_\infty^{(molar)}$ [mol/(m$^2$s)] of various gases as a function of the sticking coefficient $\alpha_{SC}$ for thermal accommodation coefficient $\alpha_{TAC}$ = [1,0.8,0.2] with $P_\infty$ = 0.1 Pa, $T_\infty$ = 300 K and $\tau_W$ = 0.05.

higher adsorption molar flow rate is sustained as the gas becomes lighter. Also, the net molar flux is directly proportional to the reference pressure $P_\infty$. In that sense following the demonstration procedure shown here the dimensionless results of the previous subsection can be readily applied in a wide range of reference conditions and various gases for comparison with experiments and other practical purposes.

## 4. Concluding remarks

The steady one-dimensional half-space flow of a monatomic gas in the presence of an absorbing planar wall is investigated based on the direct solution of the BGK kinetic model equation. The involved flow parameters include the sticking $\alpha_{SC}$ and thermal accommodation $\alpha_{TAC}$ coefficients, the ratio of the surface temperature over the far upstream temperature $\tau_W$ and the upstream normalized velocity $u_\infty$. The problem is properly defined only when three out of the four involved parameters are given. Particular attention is given on the effect of the value of $\alpha_{TAC}$ on $u_\infty$, as well as on the half space macroscopic distribution of density, velocity, temperature and pressure, for various prescribed values of $\alpha_{SC}$ and $\tau_W$. It has been found that as the thermal accommodation of the gas on the surface is reduced the adsorbing flux is also reduced or otherwise for a prescribed adsorbing flux the sticking coefficient must be increased. Furthermore, the effect of partial thermal accommodation is enlarged as the difference, between the surface temperature and the far upstream temperature, is increased. Overall, the effect of $\alpha_{TAC}$ is significant in all flow quantities and the type of thermal gas-surface interaction must be accordingly taken into consideration. It is hoped that the present work will support further investigation on the estimation of the sticking coefficients and cryopump modeling via comparison with experimental works.

## Acknowledgments

Part of this work has been carried out within the framework of the EUROfusion Consortium and has received funding from the Euratom Research and Training Programme 2014–2018 under grant agreement No 633053 (WP TFV). The views and opinions expresses herein do not necessarily reflect those of the European Commission. A part of this work was carried out using the HELIOS supercomputer system at Computational Simulation Centre of International Fusion Energy Research Centre (IFERC-CSC), Aomori, Japan, under the Broader Approach collaboration between Euratom and Japan, implemented by Fusion for Energy and JAEA.

## Appendix A. Supplementary data

Supplementary data related to this article can be found at http://dx.doi.org/10.1016/j.vacuum.2015.12.002.

## Appendix. Conservation equations

Equation (14) is multiplied successively by 1, and $c_x$ and the resulting equations are integrated over the molecular velocity space to yield, the following conservation equations:

$$\text{Mass}: \quad \frac{\partial}{\partial x}(nu) = 0 \tag{A1}$$

$$x - \text{momentum}: \frac{\partial}{\partial x}\left(p_{xx} + nu^2\right) = 0 \tag{A2}$$

Similarly, operating on equation (14) by $\int c_x^2(\cdot)dc_x$ and $\int(\cdot)\,dc_x$ respectively and following some typical manipulations the energy conservation equation is obtained:

$$\text{Energy}: \quad \frac{\partial}{\partial x}\left[nu\left(u^2 + \frac{3\tau}{2}\right) + 2up_{xx} + q_x\right] = 0 \tag{A3}$$

The above conservation equations are applied to benchmark the accuracy of the numerical scheme.

## References

[1] C. Cercignani, The Boltzmann Equation and its Applications, Springer-Verlag, Berlin, 1988.
[2] G.A. Bird, Molecular Gas Dynamics and the Direct Simulation of Gas Flows,

Clarendon Press, Oxford, 1994.
[3] K. Jousten, Handbook of Vacuum Technology, Wiley-VCH Verlag, Weinheim, Germany, 2008.
[4] C. Day, A. Schwenk-Ferrero, Sticking coefficients for helium and helium-containing mixtures at activated carbon under liquid helium cooling conditions, Vacuum 53 (1999) 253–256.
[5] C. Day, A. Antipenkov, M. Dremel, H. Haas, V. Hauer, A. Mack, D.K. Murdoch, M. Wykes, R&D and design for the cryogenic and mechanical vacuum pumping systems of ITER, Vacuum 81 (2007) 738–747.
[6] S. Varoutis, C. Day, Numerical modeling of an ITER type cryopump, Fusion Eng. Des. 87 (2012) 1395–1398.
[7] M. Kovari, R. Clarke, T. Shephard, Compound cryopump for fusion reactors, Fusion Eng. Des. 88 (2013) 3293–3298.
[8] A. Frezzotti, G.P. Ghiroldi, L. Gibelli, Rarefied gas mixtures flows driven by surface absorption, Vacuum 86 (2012) 1731–1738.
[9] A. Frezzotti, G.P. Ghiroldi, L. Gibelli, DSMC simulation of rarefied gas mixtures flows past arrays of absorbing plates, Vacuum 103 (2014) 57–67.
[10] W.M. Trott, J.N. Castaneda, J.R. Torczynski, M.A. Gallis, D.J. Rader, An experimental assembly for precise measurement of thermal accommodation, Rev. Sci. Instrum. 82 (0355120) (2011).
[11] Y.G. Semyonov, S.F. Borisov, P.E. Suetin, Investigation of heat transfer in rarefied gases over a wide range of Knudsen numbers, Int. J. Heat Mass Transf. 27 (10) (1984) 1789–1799.
[12] H. Yamaguchi, K. Kanazawa, Y. Matsuda, T. Niimi, A. Polikarpov, I. Graur, Investigation on heat transfer between two coaxial cylinders for measurement of thermal accommodation coefficient, Phys. Fluids 24 (062002) (2012).
[13] S. Song, M.M. Yovanovich, Correlation of thermal accommodation coefficient for engineering surfaces, ASME HTD Vol. 69 (1987) 107–116.
[14] J.C. Haas, V.S. Arpaci, G.S. Springer, Mass and heat transfer in a diatomic gas, J. Plasma Phys. 6 (1971) 547–560.
[15] C. Tantos, D. Valougeorgis, A. Frezzotti, Conductive heat transfer in rarefied polyatomic gases confined between parallel plates via various kinetic models and the DSMC method, Int. J. Heat Mass Transf. (2015) 636–651.
[16] P.L. Bhatnagar, E.P. Gross, M.A. Krook, A model for collision processes in gases. I. Small amplitude processes in charged and neutral one-component systems, Phys. Rev. 94 (1954) 511–525.
[17] P. Wellander, On the temperature jump in a rarefied gas, Ark. Fys. 7 (1954) 507–553.
[18] I. Graur, A. Ph. Polikarpov, F. Sharipov, Numerical modeling of rarefied gas flow through a slit into vacuum based on the kinetic equation, Comput. Fluids 49 (2011) 87–92.
[19] F. Sharipov, Benchmark problems in rarefied gas dynamics, Vacuum 86 (2012) 1697–1700.
[20] K. Aoki, K. Nishino, Y. Sone, H. Sugimoto, Numerical analysis of steady flows of a gas condensing on or evaporating from its plane condensed phase on the basis of kinetic theory: effect of gas motion along the condensed phase, Phys. Fluids A 3 (9) (1991) 2260–2275.
[21] F. Sharipov, V. Seleznev, Data on internal rarefied gas flows, J. Phys. Chem. Ref. Data 27 (3) (1998) 657–706.
[22] S. Pantazis, D. Valougeorgis, Heat transfer between parallel plates via kinetic theory in the whole range of the Knudsen number, in: Paper 407, 5th European Thermal-Sciences Conference, 19–22/5/2008, Eindhoven, Netherlands, 2008.
[23] S. Pantazis, D. Valougeorgis, Non-linear heat transfer through rarefied gases between coaxial cylindrical surfaces at different temperatures, Eur. J. Mech. B/Fluids 29 (2010) 494–509.
[24] W.G. Baechler, Cryopumps for research and industry, Vacuum 37 (1987) 21–29.
[25] H. Haas, C. Day, D. Valougeorgis, S. Naris, C. Tantos, Design Assessment Studies DAS05-T02: Further Examination of Isotope Separation in a Cryopump, 2013. Report for TAWP13-DAS05-D02.
[26] L.H. Holway, New statistical models for kinetic theory: methods of construction, Phys. Fluids 9 (9) (1966) 1658–1673.